HAL
open science

Colossal permittivity and low losses in Ba1–xSrxTiO3–δ reduced nanoceramics

Sébastien Dupuis, Soumitra Sulekar, Ji Hyun Kim, Hyuksu Han, Pascal Dufour, Christophe Tenailleau, Juan Claudio Nino, Sophie Guillemet-Fritsch

To cite this version:

Sébastien Dupuis, Soumitra Sulekar, Ji Hyun Kim, Hyuksu Han, Pascal Dufour, et al.. Colossal permittivity and low losses in Ba1–xSrxTiO3–δ reduced nanoceramics. Journal of the European Ceramic Society, 2016, 36 (3), pp.567-575. 10.1016/j.jeurceramsoc.2015.10.017 . hal-02134637

HAL Id: hal-02134637

https://hal.science/hal-02134637v1

Submitted on 20 May 2019

HAL is a multi-disciplinary open access archive for the deposit and dissemination of scientific research documents, whether they are published or not. The documents may come from teaching and research institutions in France or abroad, or from public or private research centers.

L'archive ouverte pluridisciplinaire **HAL**, est destinée au dépôt et à la diffusion de documents scientifiques de niveau recherche, publiés ou non, émanant des établissements d'enseignement et de recherche français ou étrangers, des laboratoires publics ou privés.

Open Archive Toulouse Archive Ouverte (OATAO)

OATAO is an open access repository that collects the work of some Toulouse researchers and makes it freely available over the web where possible.

This is an author's version published in: https://oatao.univ-toulouse.fr/19783

Official URL: http://dx.doi.org/10.1016/j.jeurceramsoc.2015.10.017

To cite this version :

Dupuis, Sébastien and Sulekar, Soumitra and Kim, Ji Hyun and Han, Hyuksu and Dufour, Pascal and Tenailleau, Christophe and Nino, Juan Claudio and Guillemet-Fritsch, Sophie Colossal permittivity and low losses in Ba1−xSrxTiO3−δ reduced nanoceramics. (2016) Journal of the European Ceramic Society, vol. 36 (n° 3). pp. 567-575. ISSN 0955-2219

Any correspondence concerning this service should be sent to the repository administrator: tech-oatao@listes-diff.inp-toulouse.fr

Colossal permittivity and low losses in $Ba_{1-x}Sr_xTiO_{3-\delta}$ reduced nanoceramics

Sébastien Dupuis [a], Soumitra Sulekar [b], Ji Hyun Kim [b], Hyuksu Han [a,c], Pascal Dufour [a], Christophe Tenailleau [a], Juan Claudio Nino [b], Sophie Guillemet-Fritsch [a,*]

[a] CNRS, Institut Carnot CIRIMAT, UMR CNRS-UPS-INP 5085, Université Paul-Sabatier, 118 route de Narbonne, 31062 Toulouse Cedex 9, France
[b] Department of Materials Science and Engineering University of Florida, Gainesville, FL 32611, USA
[c] Korea Institute of Industrial Technology (KITECH), 137-41 Gwahakdanji-ro, Gangneung-si, Gangwon-do 25440, Republic of Korea

A B S T R A C T

The oxalate route offers a controlled approach to synthesize pure $Ba_{1-x}Sr_xTiO_3$ (BST) ($0 \leq x \leq 1$) nanoparticles ($\phi \approx 150$ nm in diameter). Reduced BST dense nanoceramics were obtained by spark plasma sintering (SPS) and then annealed for a short time to reach colossal permittivity ($\epsilon'_r = 10^5$) with low dielectric losses ($\tan\delta = 0.03$) at 1 kHz and 300 K. The effects of Ba–Sr substitution on structural, microstructural and electrical properties were analyzed. Comprehensive analysis of the electrical properties indicates that polaron hopping, mediated by Ti^{3+} ions and oxygen vacancies is the main contributing mechanism to colossal permittivity in Ba-rich BST compounds. Substitution of Ba by Sr reduced the contribution of polaron hopping and led to a decrease of real and imaginary parts of permittivity, while preserving interfacial polarization and yielding better temperature stability. The lowest temperature coefficient of capacitance, or TCC (variation of capacitance between 310 K and 450 K) value, i.e., 44 ppm K^{-1}, is obtained for $SrTiO_3$.

Keywords:
Barium strontium titanate
Colossal permittivity
Spark plasma sintering
Nanoceramic
Dielectric properties

1. Introduction

Barium strontium titanate ($Ba_{1-x}Sr_xTiO_3$, BST) is an intensively studied and well-known solid solution for various electronic applications such as capacitors [1,2], positive temperature coefficient resistors [3], phase shifters [4], and gas sensors [5]. BST compounds are synthesized through a variety of methods like coprecipitation [6,7], sol–gel synthesis [8], hydrothermal [9], and solid-state [10] reactions. When conventionally sintered, BST bulk ceramics show high relative permittivity with low losses ($\epsilon'_r = 10^3$ and $\tan\delta = 0.03$) and a variable Curie temperature [11,12].

Since the turn of the century, there has been renewed interest in compounds with colossal effective permittivity elicited by manipulation of extrinsic polarization mechanisms [13–17]. Then, in order to better understand the origin of colossal permittivity, a number of researchers have analyzed electrical behavior of these materials. Recently, fast firing processes, such as spark plasma sintering (SPS) or microwave sintering, were employed to achieve colossal permittivity in BT based ceramics [6,18–20]. In these fast-fired materials, mixed valence state of the cations due to extrinsic defects, localized in the vicinity of grain boundaries, was proposed as a mechanism at the origin of colossal permittivity [21,22]. In addition, it was shown that semi-conductive grains are separated by thin insulating grain boundaries, leading to internal barrier layer effect (IBLC) for colossal permittivity in BT [21–23]. The properties of BT can be easily tuned by the substitution of Ba^{2+} by Sr^{2+} cations. The aim of this paper is to understand the effect of Ba–Sr substitution on the dielectric properties of a series of $Ba_{1-x}Sr_xTiO_3$ ($0 \leq x \leq 1$) solid solutions.

2. Experimental procedure

2.1. Powder synthesis and spark plasma sintering

BST ($0 \leq x \leq 1$) nanopowders were synthesized by an oxalate coprecipitation route. The procedure is described in a previous paper [24] and the same procedure was used in this work. Briefly, $BaCl_2 \cdot 2H_2O$ (Prolabo), $SrCl_2 \cdot 6H_2O$ (Aldrich) and lab-made $TiOCl_2$ solution (15 wt.% of Ti) were used as precursors. The precursors were weighed in appropriate proportions to control the powder stoichiometry, dissolved in water and added to an ethanolic oxalic acid solution. The solution was stirred and aged for 5 h, then centrifuged and dried overnight at 80 °C. The oxide powders were obtained after calcination at 850 °C for 4 h in static air.

To densify the BST nanopowders, SPS was carried out using a Dr. Sinter 2080 device from Sumitomo Coal Mining (Fuji Electronic

* Corresponding author. Fax: +33 561556163.
E-mail address: guillem@chimie.ups-tlse.fr (S. Guillemet-Fritsch).

http://dx.doi.org/10.1016/j.jeurceramsoc.2015.10.017

Industrial, Saitama, Japan). The same processing parameters were used for all the compositions. The sintering procedure has been optimized in previous work [24]. Briefly, 0.5 g of each batch was loaded in an 8-mm-inner-diameter graphite die. A sheet of graphite paper was inserted between the punch and the powder as well as between the die and the powder for easy removal of the pellet after sintering. Powders were sintered in vacuum (residual cell pressure <10 Pa). A pulse pattern of twelve current pulse periods followed by two periods of zero current was used. A heating rate of 25 °C/min was used from 600 to 1150 °C, where a 3-min dwell time at the sintering temperature was applied. An optical pyrometer focused on a small hole at the surface of the die was used to measure and monitor the temperature. A uniaxial pressure of 75 MPa was applied for 2 min before reaching the dwell temperature. After the 3-min dwell, the electric current was switched off and the pressure was released. In situ dilatometry-based shrinkage curves for the different powders were recorded during the sintering process. The as-sintered pellets showed a thin carbon layer on the surface due to graphite contamination from the graphite sheets. This layer was removed by polishing the surface. In a previous work [18], the presence of residual carbon due to SPS processing technique was determined through the spectrometric quantification of CO_2 and appeared to be very low with a concentration of 93 ppm. Samples appeared dark blue, consistent with the presence of Ti^{3+} caused by the reducing atmosphere used during SPS (low vacuum and carbon environment) as previously demonstrated using X-ray photoelectron spectroscopy (XPS) [25]. SPS pellets were finally annealed for 15 min at 850 °C in an oxidizing atmosphere in an attempt to partially restore the oxygen stoichiometry.

2.2. Material characterization

The chemical composition of the different oxide powders was determined using inductively coupled plasma-atomic emission spectroscopy (ICP-AES) with a JY 2000 device (Horiba Jobin Yvon, Kyoto, Japan). The morphology of the powders was observed with a field emission gun scanning electron microscope (FEG-SEM, JSM 6700F, JEOL, Tokyo, Japan) and the particle size was determined by ImageJ software [26]. The grain boundaries thicknesses were observed with a high resolution transmission electron microscope (HRTEM, JEM 2100F, JEOL, Tokyo, Japan). The crystalline structure was investigated by X-ray diffraction analysis using a D4 Endeavor X-ray diffractometer ($CuK\alpha_1$ = 0.154056 nm and $CuK\alpha_2$ = 0.154044 nm; Bruker AXS, Karlsruhe, Germany) from 20° to 80° (2-theta). The density of the pellets was determined by the Archimedes method using an ARJ 220-4M balance (KERN, Murnau-Westried, Germany). Prior to electrical measurements, the ceramic disks were coated with thin gold electrodes (thickness ~30 nm) by sputtering (108 Auto, Cressington Scientific Instruments, Watford, U.K.). The relative permittivity and the dielectric losses were obtained from impedance measurements using a 4294A Precision Impedance Analyzer (Agilent Technologies, Palo Alto, CA) in the range of 40–100 kHz at room temperature and an applied ac voltage of 1 V. For temperature dependence of the dielectric properties, the electroded samples were placed in a closed cycle cryogenic workstation (CTI 22, Cryo Industries of America, Manchester, NH) and measurements were taken as a function of temperature (40–300 K) using an Agilent 4284A LCR meter.

3. Results and discussion

3.1. Microstructure, X-ray diffraction and density

Fig. 1 shows the FEG-SEM images of the starting powders. The morphology of the particles is roughly homogeneous and transforms from a spherical shape for $BaTiO_3$ (BT) to a cubic shape for pure $SrTiO_3$ (ST). The average particle size decreases as the strontium content increases, from 150 ± 40 nm for BT to 80 ± 20 nm for ST.

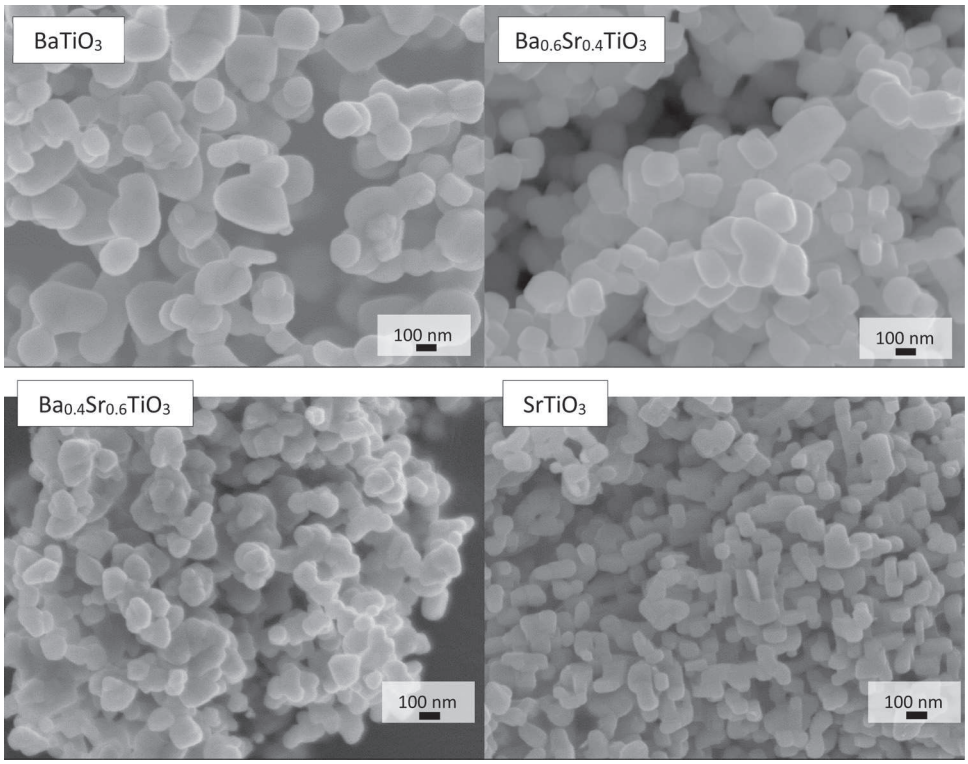

Fig. 1. FEG-SEM micrographs of $Ba_{1-x}Sr_xTiO_3$ powders.

Table 1
Grain size of the powders and ceramics, structure, lattice parameters and density of the $Ba_{1-x}Sr_xTiO_{3-\delta}$ samples.

Composition	Particle size (nm)	Ceramic grain size (nm)	Powder structure	Ceramic structure	Lattice parameters (Å)	Density (densification%)
$BaTiO_{3-\delta}$	150	240	T + C	T + C	$a = 3.9938 \pm 0.0003$ $c = 4.0295 \pm 0.0003$	5.90 (98.0)
$Ba_{0.8}Sr_{0.2}TiO_{3-\delta}$	130	180	T + C	T + C	$a = 3.9771 \pm 0.0005$ $c = 3.9883 \pm 0.0005$	5.79 (99.2)
$Ba_{0.6}Sr_{0.4}TiO_{3-\delta}$	120	130	C	C	$a = 3.9700 \pm 0.0002$	5.60 (98.9)
$Ba_{0.4}Sr_{0.6}TiO_{3-\delta}$	110	115	C	C	$a = 3.9422 \pm 0.0005$	5.44 (99.4)
$Ba_{0.2}Sr_{0.8}TiO_{3-\delta}$	95	120	C	C	$a = 3.9220 \pm 0.0005$	5.25 (99.3)
$SrTiO_{3-\delta}$	80	500	C	C	$a = 3.9040 \pm 0.0003$	5.06 (99.0)

T : tetragonal, C : cubic.

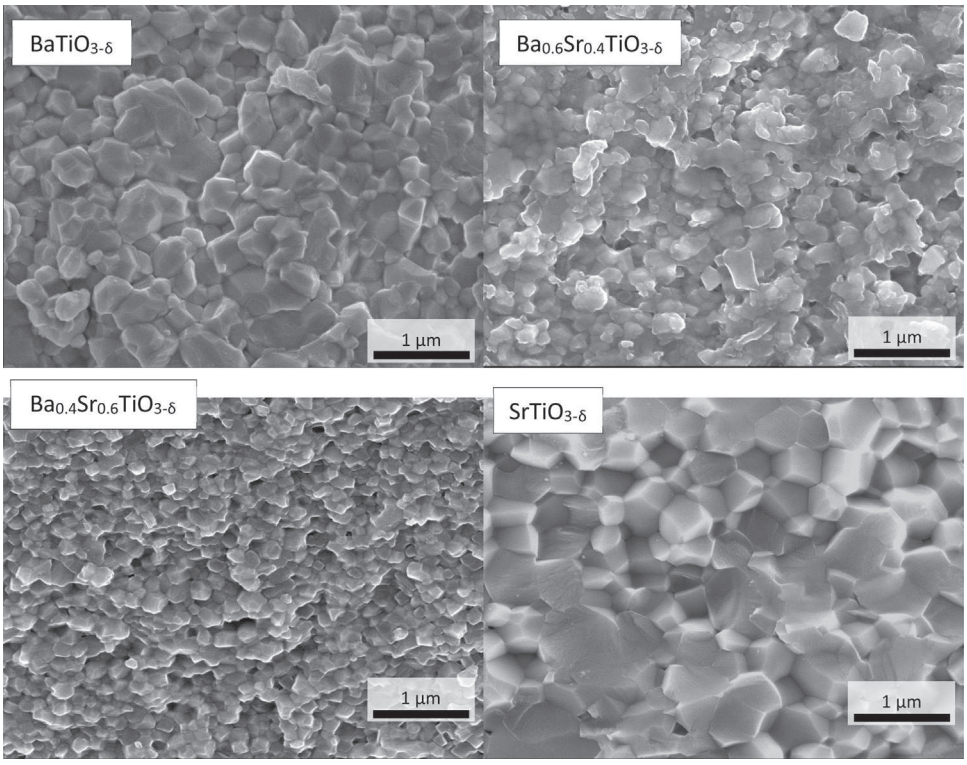

Fig. 2. FEG-SEM micrographs of $Ba_{1-x}Sr_xTiO_{3-\delta}$ fractured dense ceramics.

All the sintered ceramics had density values above 98% of theoretical (Table 1), even after a very short (3 min) sintering treatment performed at low temperature (1150 °C). The FEG-SEM images obtained from fractured surfaces of the pellets confirm little to minimal porosity as well as homogeneous microstructure (Fig. 2).

The average grain sizes were calculated using the linear intercept method (ASTM E112). They fall between 240 ± 50 nm for BT to 115 ± 15 nm for $Ba_{0.4}Sr_{0.6}TiO_{3-\delta}$ and increase to 500 ± 50 nm for ST (Table 1), indicating that moderate grain growth has occurred during sintering. These data point out that the grain growth from powder to dense ceramic is higher for ST. X-ray diffraction patterns of $Ba_{1-x}Sr_xTiO_{3-\delta}$ samples are shown in Fig. 3.

Each composition crystallizes in the perovskite structure. No secondary phase is formed. However, a mixture of cubic and tetragonal perovskite phases is evidenced, essentially by the presence of the (0 0 2) and (2 0 0) peaks, for the barium-rich compounds ($x \leq 0.2$), while only the cubic phase is observed for $x \geq 0.4$. In addition, a shift of Bragg's peaks to higher 2θ angle is observed as Ba is substituted by Sr, indicating a decrease of the cell parameters. Calculated ceramics lattice parameters are reported in Table 1. The decrease of the unit cell as the strontium content increases can be explained by the smaller crystal radius of Shannon for Sr^{2+} cations (158 pm) compared to Ba^{2+} (175 pm) [27]. The decrease of the tetragonal distortion predicted by the Goldschmidt's factor as Sr concentration increases can be quantify. Indeed, by calculating c/a, we observe a decrease of this ratio from 1.009 for $BaTiO_3$ to 1.002 for $Ba_{0.8}Sr_{0.2}TiO_3$. The structure is then cubic for further Sr contents.

3.2. Dielectric properties

The dielectric response of the BST ($0 \leq x \leq 1$) nanoceramics were investigated in the frequency range of 40–100 kHz (Fig. 4).

As can be seen in Fig. 4, colossal permittivity up to 10^5 with low dielectric losses (tan δ < 0.05) was achieved for most of the compositions ($0 \leq x \leq 0.6$). The values for ϵ'_r and tan δ measured at 1 kHz and 300 K are reported in Table 2.

It was observed that relative permittivity and dielectric losses of BST compounds gradually decreased as Sr content increased while still maintaining colossal permittivity up to 10^4 with low dielectric losses (tan δ = 0.03) for $x = 0.8$. It is worth noticing that the BST nanoceramics samples in this work exhibit much higher permittivity compared to the results in the open literature [28–33]. For instance, Fu et al. [28] prepared the solid solution $Ba_xSr_{1-x}TiO_3$

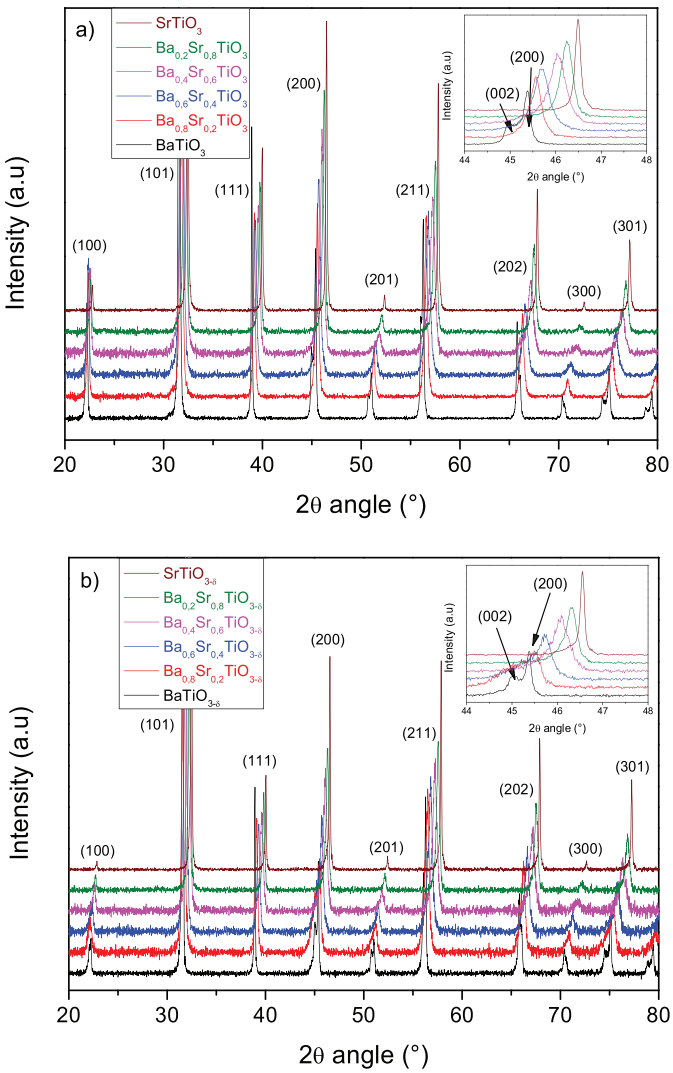

Fig. 3. XRD patterns of $Ba_{1-x}Sr_xTiO_3$ ($0 \le x \le 1$) materials (a) powders and (b) ceramics; inset: 44–60° 2θ angle enlargement.

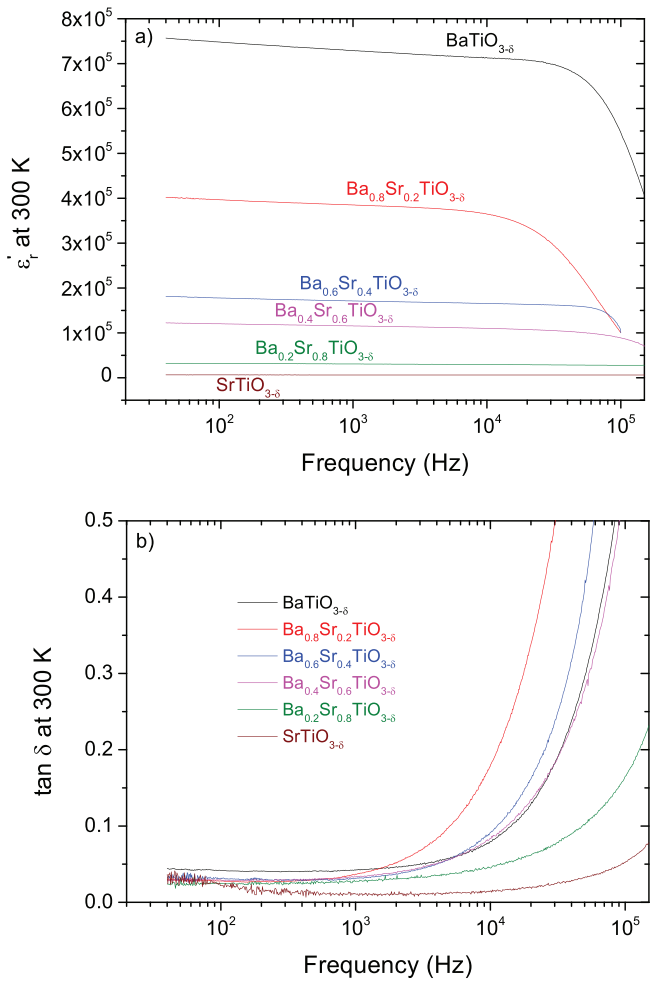

Fig. 4. Variation of the real part of relative permittivity (a) and losses (b) as a function of frequency for the $Ba_{1-x}Sr_xTiO_{3-\delta}$ nanoceramics at 300 K.

Table 2
Dielectric properties of the $Ba_{1-x}Sr_xTiO_{3-\delta}$ nanoceramics.

Composition	ϵ'_r(1 kHz, 300 K)	tan δ (1 kHz, 300 K)	TCC (10^{-3} K^{-1})
$BaTiO_{3-\delta}$	729 000	0.05	1.9
$Ba_{0.8}Sr_{0.2}TiO_{3-\delta}$	388 000	0.04	1.5
$Ba_{0.6}Sr_{0.4}TiO_{3-\delta}$	174 000	0.03	3.6
$Ba_{0.4}Sr_{0.6}TiO_{3-\delta}$	115 000	0.03	3.3
$Ba_{0.2}Sr_{0.8}TiO_{3-\delta}$	30 800	0.03	0.5
$SrTiO_{3-\delta}$	6 300	0.01	0.04

ceramics through solid-state reaction followed by conventional sintering. They reported permittivity values, at room temperature and for 1 kHz, ranging between 1500–3000 for increasing barium content. The combination of mechanosynthesis and spark plasma sintering has been used for the first time for the Ba–Sr–Ti–O system by Hungria et al. [31]. While the ceramics exhibited nanosize grains, low permittivity values were observed, 1400 for $BaTiO_3$ and 200 for $SrTiO_3$ respectively. Gao et al. [33] used an organosol synthesis to prepare $Ba_{0.6}Sr_{0.4}TiO_3$ nanoparticles with average grain size of 35 nm. The authors used spark plasma sintering to prepare nanoceramics showing a maximum permittivity value of 3000.

These examples show the importance of each step of the ceramic process which were controlled in our work to obtain colossal permittivity values in the BST ceramics: oxalate coprecipitation to synthesize homogeneous powder of controlled morphology, size and stoichiometry, SPS sintering to obtain ceramics with nanosize grains and reduced titanium cations and a short annealing treatment to retain oxygen sub-stoichiometric compounds.

The permittivity and the losses of BST compounds as a function of temperature (300–450 K) are shown in Fig. 5. Colossal permittivity is observed over a wide temperature range (300–450 K). The ferroelectric–paraelectric transition, corresponding to the tetragonal–cubic phase transition is seen only for pure BT ceramics by a peak of ϵ'_r occurring at the same temperature (T_c = 396 K) whatever the frequency until 100 kHz.

The temperature coefficient of capacitance, TCC (variation of capacitance between 310–450 K), is determined according to Eq. (1):

$$TCC = \frac{1}{C(310K)} \times \frac{C(\max) - C(\min)}{450K - 310K} \quad (1)$$

The lowest value of TCC, 44 ppm K^{-1}, observed for the composition $SrTiO_{3-\delta}$ (Table 2), is lower than the values reported for temperature stable capacitors, i.e., in the $BaTiO_3$-$Bi(Zn_{1/2}Ti_{1/2})O_3$-$BiScO_3$ system [6]. In the following sections, we will discuss about more details for the possible mechanisms, explaining the temperature stable dielectric properties of BST compounds by using corresponding physical models such as Debye relaxation, universal dielectric response (UDR), and hopping polarization models.

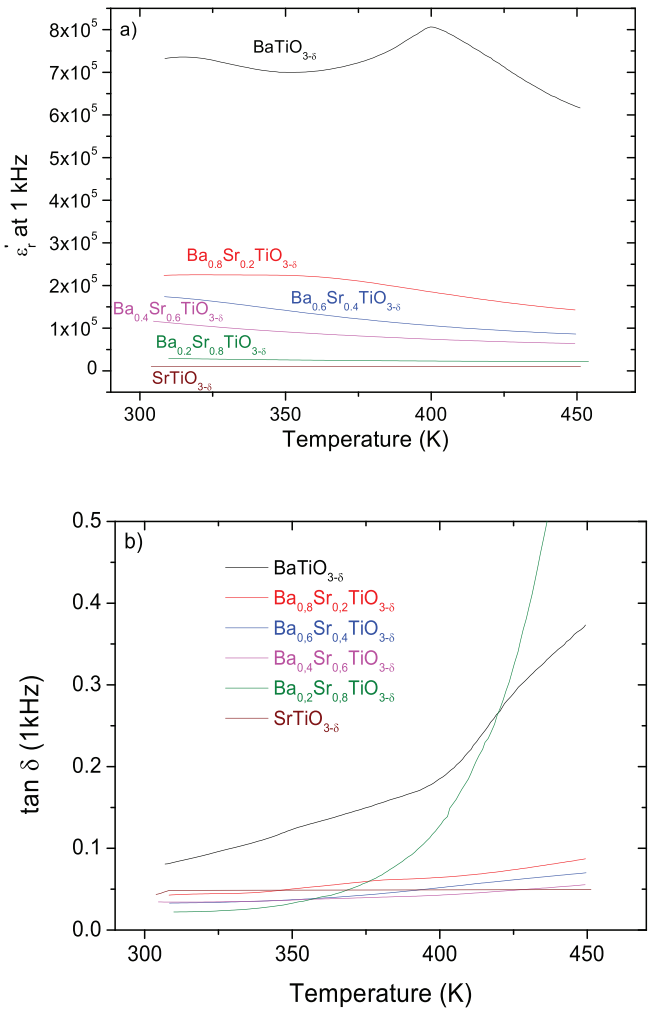

Fig. 5. Variation of the real part of the relative permittivity (a) and losses (b) as a function of temperature measured at 1 kHz for the $Ba_{1-x}Sr_xTiO_{3-\delta}$ nanoceramics.

3.3. Polarization mechanisms in BST compounds

To investigate the relaxation phenomena observed in BST nanoceramics, the dielectric properties of each composition were measured as a function of temperature (40–300 K) at different frequencies. Fig. 6 shows the dielectric data for one Ba-rich ($x = 0.2$) and one Sr-rich composition ($x = 0.8$), respectively, which exhibit distinctly different dielectric relaxation behavior.

Debye-like dielectric relaxations were observed for both compositions, and the maximum of ϵ''_r shifts to higher temperature as frequency increases, indicating frequency dependent relaxation process may exist in the compounds. In the Debye model, the relaxation frequency and the activation energy can be extracted by using the equation below:

$$\nu = \nu_0 \exp\left(\frac{-E_A}{k_B T}\right) \tag{2}$$

where ν_0, k_B, and E_A are the pre-exponential factor, the Boltzmann constant, and the activation energy for relaxation, respectively. As such, the relaxation temperatures at different frequencies were extracted from the maximum of ϵ''_r for each of the BST compounds and plotted in the Arrhenius form to determine the activation energy

It can be clearly seen in Fig. 7 that $Ba_{0.8}Sr_{0.2}TiO_{3-\delta}$ shows two different slopes corresponding to two activation energies, while distinct slope change was not observed for $Ba_{0.2}Sr_{0.8}TiO_{3-\delta}$. This result indicates that, similar to BT [22], BST compounds with high barium content might have two different polarization mechanisms, possibly hopping polarization combined with interfacial space charge polarization, while Sr-rich BST might have only one polarization mechanism.

It is also well known that Jonscher's UDR model can be applied to explain dielectric polarization in colossal permittivity materials, which can be described by the following equations [34],

$$\epsilon'_r = \frac{\tan\left(\frac{s\pi}{2}\right) f^{s-1}\sigma_0}{\epsilon_0}$$

$$f\epsilon'_r = A(T) f^s \tag{3}$$

where σ_0 and s represent the temperature dependent constants, ϵ_0 and f are the permittivity of free space and experimental frequency ($f = \omega/2\pi$), respectively, and $A(T)$ is equal to $\left\{\tan\left(s\pi/2\right)\ \sigma_0\ \epsilon_0\right\}$. Thus, one can extract the value of the exponent s by plotting $\log(\epsilon'_r \times f)$ vs. $\log(f)$. It should be mentioned here that a s value as closer to 1 implies that the polarization charges are more highly localized [35].

Fig. 8 shows the real and imaginary parts of dielectric permittivity for BST ($x = 0.2$) and BST ($x = 0.8$) samples as a function of frequency (40–100 kHz) at different temperatures (40–300 K). Dielectric relaxation has occurred at each temperature, given that distinct relaxation peaks of imaginary part of permittivity were observed for the compositions. Furthermore, the relaxation peaks shift to lower frequencies as temperature decreases, which indicates that thermally activated relaxation phenomena is involved in the material.

Fig. 9 presents $(\epsilon'_r \times f)$ vs. f plots in log–log scales for the same samples. For the Ba-rich BST ($x = 0.2$) compound, high temperature slope is close to 1, which is different from the value of the low temperature slope, indicating that dielectric polarization is more localized at high temperature region.

As we mentioned in the previous work [22], the slope change in $\log(\epsilon'_r \times f)$ vs. $\log(f)$ plot as temperature decreases is associated with the hopping polarization which becomes inactive at lower temperatures due to insufficient energy to overcome energy barrier for polarization. However, for the Sr-rich BST compound ($x = 0.8$), no slope change was observed for the different temperature regions. Thus, one can expect that hopping polarization might not be present in Sr-rich BST compounds.

To further investigate this possibility, it is important to recall the thermally activated hopping polaron (THP) model [36], where the maximum of ϵ''_r is proportional to the number of polarons participating in hopping polarization by,

$$\epsilon''_{r\,max} = \frac{N\mu^2}{3k_B T} \tag{4}$$

$$N = N_0 \ \exp\left(-\frac{E_A}{k_B T}\right) \tag{5}$$

N and μ represent the number of hopping polarons and the hopping dipole moment respectively. N_0 and E_A are the pre-exponential factor and the activation energy related with relaxation of hopping dipoles respectively. By substituting Eq. (4) into Eq. (3), equation for the thermally activated hopping polaron model can be obtained as,

$$T\epsilon''_{max} = \left(\frac{N_0\ \mu^2}{3k_B}\right) \exp\left(-\frac{E_A}{k_B T}\right) \tag{6}$$

Thus, activation energy for hopping polarization can be calculated from the $\ln(\epsilon''_{max} \times T)$ vs. $1/T$ plot.

Fig. 10 shows $\ln(\epsilon''_{max} \times T)$ vs. $1/T$ plots for BST compounds ($x = 0.2$ and 0.8). Activation energies are extracted from the fitting results. It should be noted that, if hopping polarization is present in

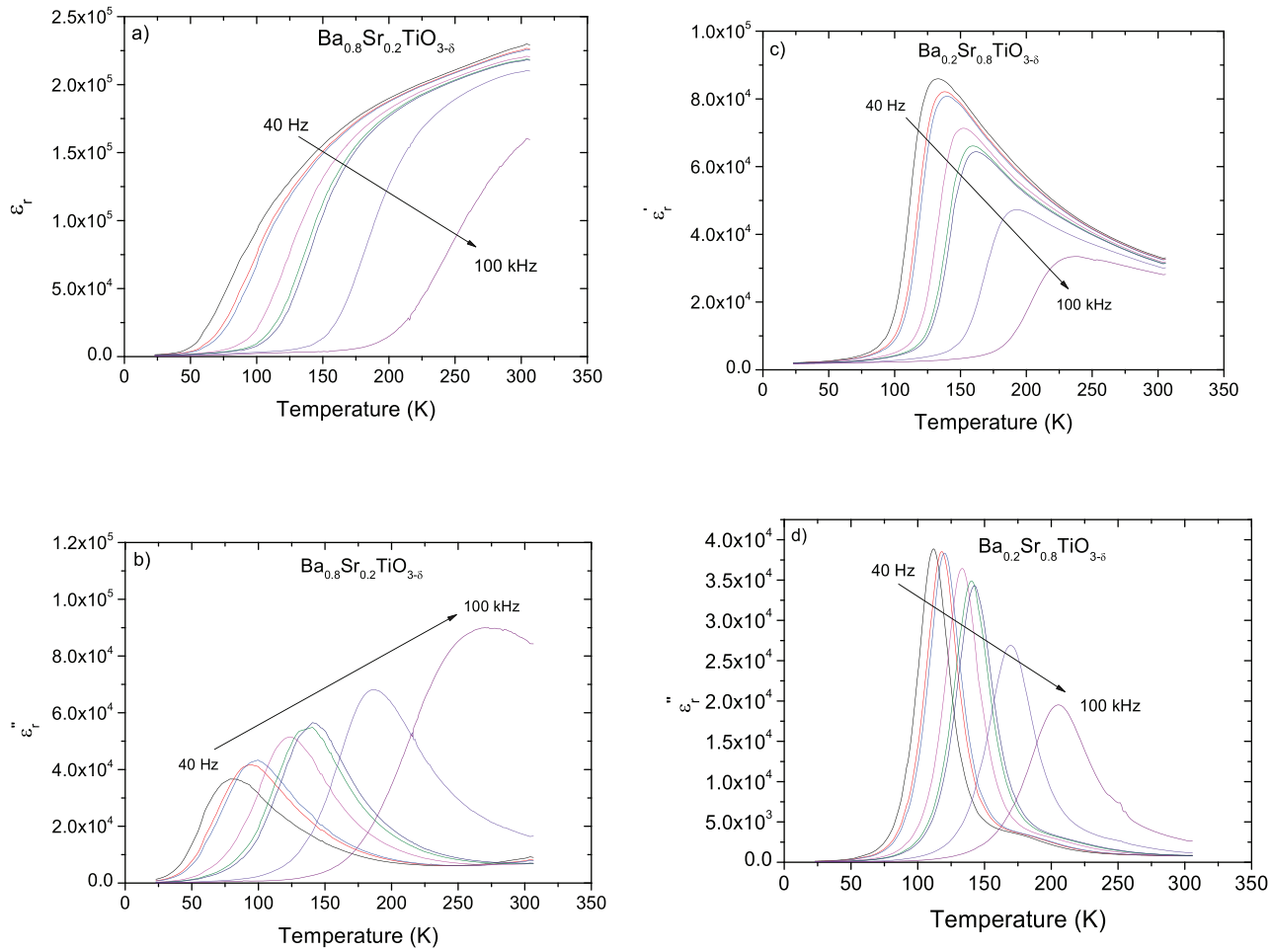

Fig. 6. Variation of the real parts (a) and (c) and the imaginary parts (b) and (d) of permittivity as a function of temperature and at different frequencies for $Ba_{0.8}Sr_{0.2}TiO_{3-\delta}$ and $Ba_{0.2}Sr_{0.8}TiO_{3-\delta}$ nanoceramics.

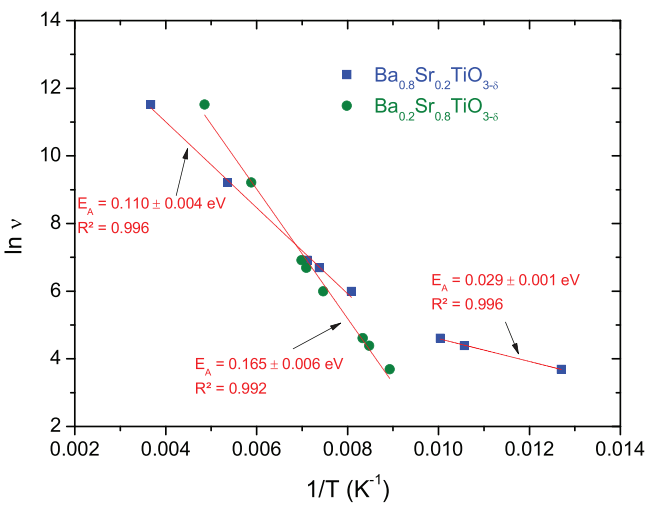

Fig. 7. Temperature dependence of relaxation frequency for $Ba_{0.8}Sr_{0.2}TiO_{3-\delta}$ and $Ba_{0.2}Sr_{0.8}TiO_{3-\delta}$ nanoceramics.

colossal permittivity material, activation energy of hopping polarization at high temperature region is comparable to the difference of activation energies at high and low temperatures obtained by using Debye model (Fig. 7) [22].

This statement seems to hold true for the case of Ba-rich BST sample ($x = 0.2$), where the activation energy difference from Debye model (0.081 eV) is well comparable with the activation energy for hopping polarization in the high temperature region (0.036 eV). However, for Sr-rich BST ($x = 0.8$), the value of $\ln(\epsilon''_{max} \times T)$ remains constant at different temperatures, indicating that no thermally activated hopping process is present in Sr-rich BST compounds (Fig. 7). Thus, one can conclude that the colossal permittivity in Ba-rich BST compounds is due to hopping polarization combined with interfacial polarization, while only interfacial polarization is responsible for Sr-rich BST compounds.

Table 3 summarizes calculated activation energy and extracted s values for BST ($x = 0.2$ and 0.8) compounds by using Debye, UDR, and THP models, respectively. The two BST compounds, Sr-rich and Ba-rich, were again selected for the analysis since those compounds exhibit most distinct dielectric properties in terms of polarization mechanisms. As observed by De Souza et al. [37,38], $BaTiO_3$ exhibits lower oxygen diffusion and surface exchange coefficients $\{D_O^*(\delta, 850\,^\circ C) = 1.2 \times 10^{-13}\,cm^2\,s^{-1}$ and $k_O^*\ (850\,^\circ C) = 3.8 \times 10^{-8}\,cm\,s^{-1}\}$ than $SrTiO_3$ $\{D_O^*(\delta,\ 850\,^\circ C) = 2.0 \times 10^{-11}\,cm^2\,s^{-1}$ and k_O^* $(850\,^\circ C) = 7.5 \times 10^{-10}\,cm\,s^{-1}\}$. Therefore, the faster diffusion of oxygen during the post annealing treatment in BST compounds, compared to BT, leads to an increase of the Ti^{3+} to Ti^{4+} oxidation rate, which results in the decrease of hopping dipole concentration in the material. Furthermore, it is well known that ferroelectricity of BST decreases as Sr content increases, and transformation from the ferroelectric phase to the paraelectric phase occurs when the Sr content increases above 0.3 [39,40]. Nanoceramics displaying colossal permittivity were achieved in BST materials, made of

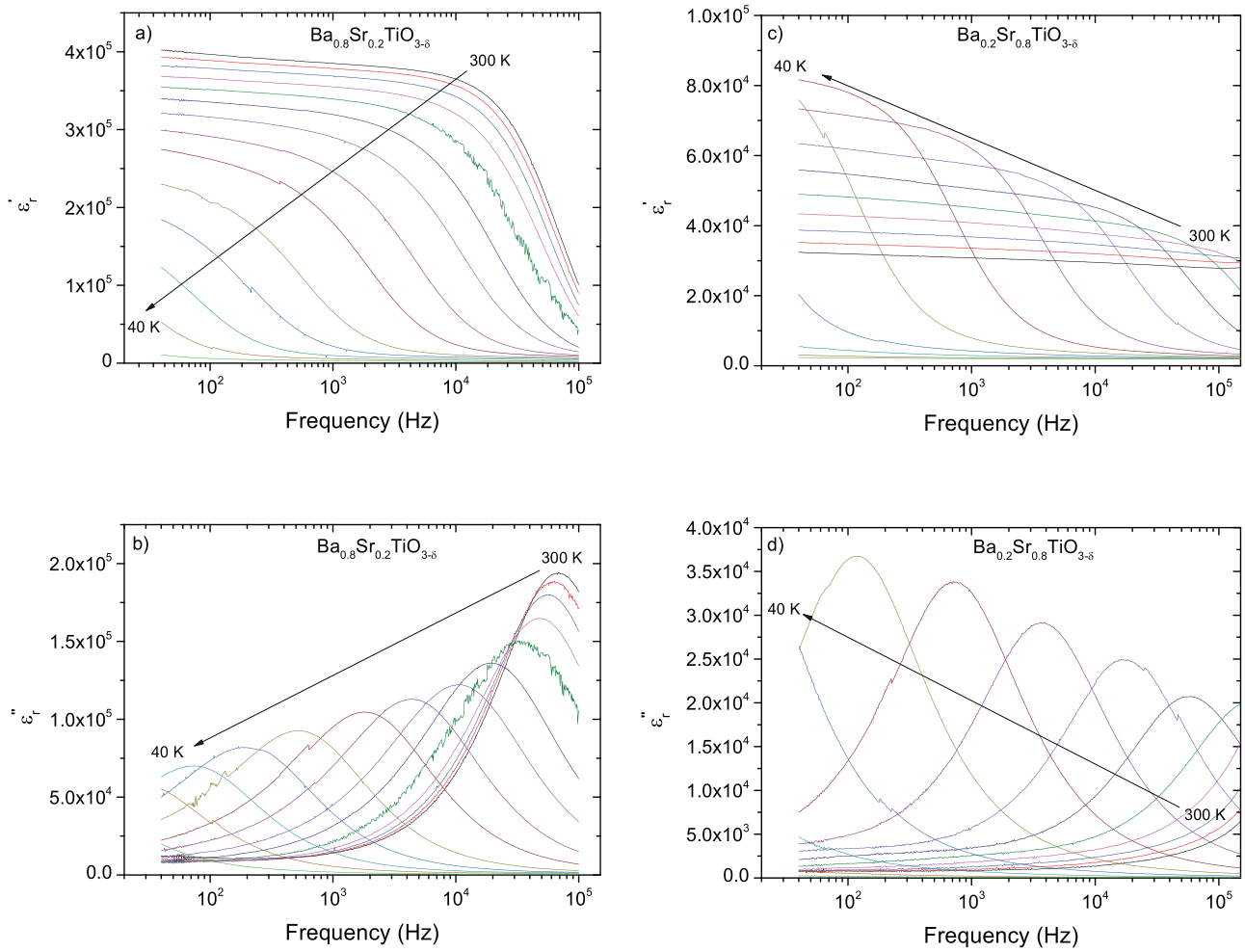

Fig. 8. Variation of the real part (a) and (c) and the imaginary part (b) and (d) of permittivity as a function of frequency and at different temperatures for $Ba_{0.8}Sr_{0.2}TiO_{3-\delta}$ and $Ba_{0.2}Sr_{0.8}TiO_{3-\delta}$ nanoceramics.

Table 3
Calculated activation energies and *s* values for BST compounds using three different analytical models.

	$Ba_{0.8}Sr_{0.2}TiO_{3-\delta}$	$Ba_{0.2}Sr_{0.8}TiO_{3-\delta}$	
Debye model(E_A, eV)	Low temp	0.029	0.165
	High temp	0.110	
UDR model (*s* value)	Low temp	0.80	0.98
	High temp	0.99	0.98
THP model (E_A, eV)	Low temp	0.015	~0
	High temp	0.036	

semiconducting grains with insulating grain boundaries. The use of ultrafine chemically homogeneous powders could lead to the fabrication of very thin dielectric films opening routes to the miniaturization and development of integrated systems. The temperature stability of the barium strontium system is observed without further dopants, which represents a great advantage for industrial applications.

The use of BST as a dielectric material provides a simple way to modulate the semi-conductive behavior of the grains and prepare capacitors with controlled colossal permittivity.

4. Conclusion

The simple coprecipitation process allows to prepare a variety of pure barium strontium titanate compounds of controlled cation stoichiometry. Synthesized nanopowders exhibit a perovskite structure based on a cubic lattice for $SrTiO_3$ and a mixture of cubic and tetragonal lattices with the increase of Ba-content. SPS sintering leads to dense nanostructured reduced ceramics which exhibit colossal permittivity values with low associated losses. The electrical properties were analyzed in detail using Debye, UDR and hopping polarons models. In Ba rich compounds, the properties are attributed to polarization mechanisms at the grain boundary interfaces and to hopping. The decrease of the permittivity value as the Sr-content increases, is due to a decrease of the hopping contribution. The composition of $Ba_{0.6}Sr_{0.4}TiO_{3-\delta}$ can be chosen as an optimal BST compound for the colossal permittivity material. It shows the highest value of ϵ'_r (174,000) and the lowest value of tan δ (0.03) over a wide temperature range. Moreover, the strontium

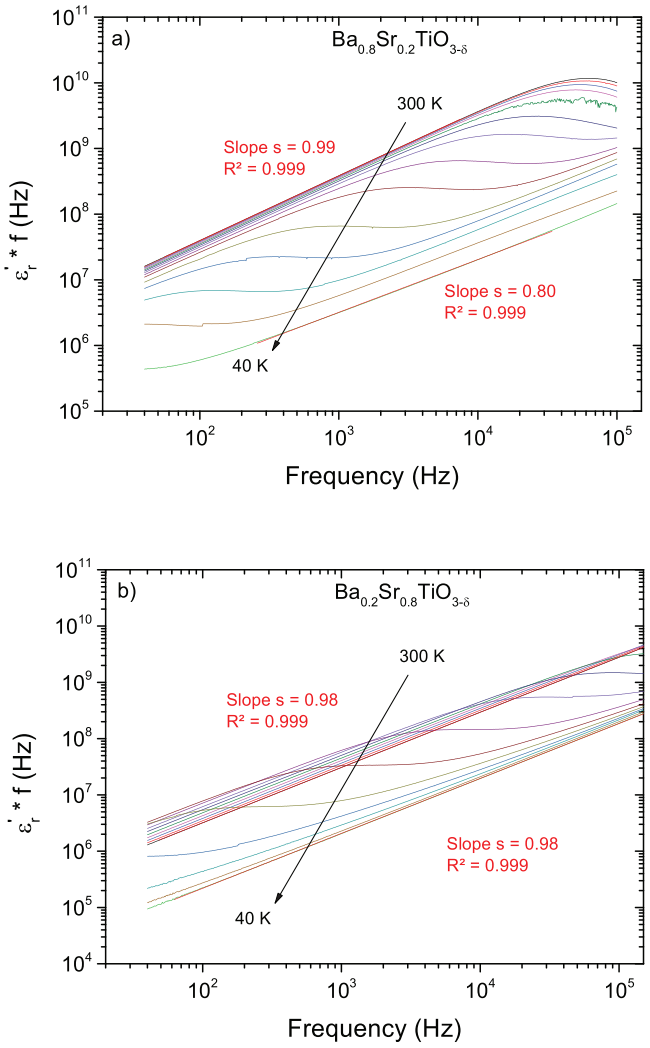

Fig. 9. $\epsilon'_r \times f$ vs. f plot in log–log scales for (a) $Ba_{0.8}Sr_{0.2}TiO_{3-\delta}$ and (b) $Ba_{0.2}Sr_{0.8}TiO_{3-\delta}$ dense nanoceramics at different temperatures (40–300 K).

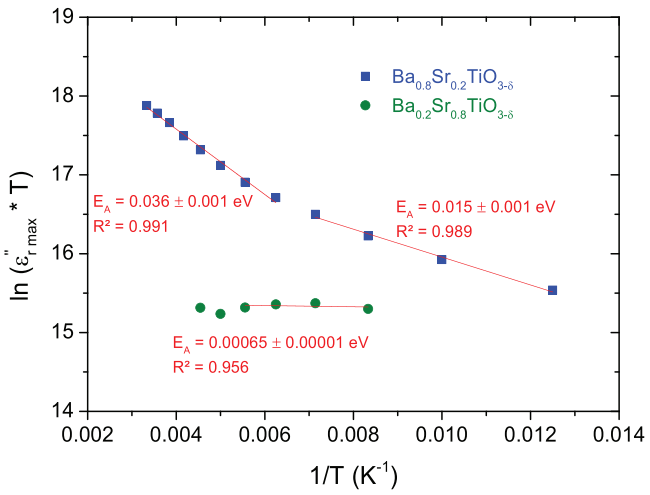

Fig. 10. Activation energy values extracted from the hopping polarons model for $Ba_{0.8}Sr_{0.2}TiO_{3-\delta}$ and $Ba_{0.2}Sr_{0.8}TiO_{3-\delta}$ nanoceramics.

rich BST reduced nanostructured ceramics exhibit temperature stable permittivity.

References

[1] L.Y. Vikki Chen, R. Forse, D. Chase, R.A. York, Analog tunable matching network using integrated thin-film BST capacitors, IEEE MTT-S Digest (2004), TUSC-6.
[2] J.H. Herbert, Ceramic Dielectrics and Capacitors, Gordon and Breach Science Publishers, New York, 1985.
[3] M. Viviani, M. Leoni, M.T. Buscaglia, V. Buscaglia, P. Nanni, Positive temperature coefficient of electrical resistivity below 150 K in barium strontium titanate, J. Am. Ceram. Soc. 87 (4) (2004) 756–758.
[4] F. Zimmermann, M. Voigts, C. Weil, R. Jakoby, P. Wang, W. Menesklou, E. Ivers-Tiffée, Investigation of barium strontium titanate thick films for tunable phase shifters, J. Eur. Ceram. Soc. 21 (2001) 2019–2023.
[5] G.H. Jain, L.A. Patil, P.P. Patil, U.P. Mulik, K.R. Patil, Studies on gas sensing performance of pure and modified barium strontium titanate thick film resistors, Bull. Mater. Sci. 30 (1) (2007) 9–17.
[6] N. Raengthon, T. Sebastian, D. Cumming, I.M. Reaney, D. Cann, $BaTiO_3$-$Bi(Zn_{1/2}Ti_{1/2})O_3$-$BiScO_3$ ceramics for high temperature capacitor applications, J. Am. Ceram. Soc. 95 (11) (2012) 3554–3561.
[7] Y.B. Khollam, S.B. Deshpande, H.S. Potdar, S.V. Bhoraskara, S.K. Sainkar, S.R. Date, Simple oxalate precursor route for the preparation of barium–strontium titanate: $Ba_{1-x}Sr_xTiO_3$ powders, Mater. Charact. 54 (2005) 63.
[8] H. Shiibashi, M. Matsuda, H. Kuwabara, Low-temperature preparation of $(Ba,Sr)TiO_3$ perovskite phase by sol–gel method, J. Sol–Gel Sci. Technol. 16 (1999) 129–134.
[9] L. Yang, Y. Wang, Y. Wang, X. Wang, X. Wang, Facile morphology-controlled synthesis of $Ba_{1-x}Sr_xTiO_3$ ($0 \leq x < 1$) crystals via a hydrothermal method, J. Ceram. Soc. Japan 120 (1) (2012) 43–46.
[10] S.K. Rout, S. Panigrahi, Mechanism of phase formation of $BaTiO_3$–$SrTiO_3$ solid solution through solid-oxide reaction, Indian J. Pure Appl. Phys. 44 (2006) 606–611.
[11] C. Fu, C. Yang, H. Chen, Y. Wang, L. Hu, Microstructure and dielectric properties of $Ba_xSr_{1-x}TiO_3$ ceramics, Mater. Sci. Eng. B 119 (2005) 185–188.
[12] W. Li, Z. Xu, R. Chu, P. Fu, J. Hao, Sol–gel synthesis and characterization of $Ba_{(1-x)}Sr_xTiO_3$ ceramics, J. Alloys Compd. 499 (2010) 255–258.
[13] M.A. Subramanian, D. Li, N. Duan, B.A. Reisner, A.W. Sleight, High dielectric constant in $ACu_3Ti_4O_{12}$ and $ACu_3Ti_3FeO_{12}$ phases, J. Sol. State Chem. 151 (2000) 323–325.
[14] A.P. Ramirez, M.A. Subramanian, M. Gardel, G. Blumberg, D. Li, T. Vogt, S.M. Shapiro, Giant dielectric constant response in a copper–titanate, Solid State Commun. 115 (217) (2000).
[15] C.C. Homes, T. Vogt, S.M. Shapiro, S. Wakimoto, A.P. Ramirez, Optical response of high-dielectric-constant perovskite-related oxide, Science 293 (2001) 673–676.
[16] I.P. Raevski, S.A. Prosandeev, A.S. Bogatin, M.A. Malitskaya, L. Jastrabik, High dielectric permittivity in $AFe_{1/2}B_{1/2}O_3$ nonferroelectric perovskite ceramics (A = Ba, Sr, Ca; B = Nb, Ta, Sb), J. Appl. Phys. 93 (2003) 4130–4136.
[17] D. Capsoni, M. Bini, V. Massarotti, G. Chiodelli, M.C. Mozzatic, C.B. Azzoni, Role of doping and CuO segregation in improving the giant permittivity of $CaCu_3Ti_4O_{12}$, J. Solid State Chem. 177 (2004) 4494.
[18] S. Guillemet-Fritsch, Z. Valdez-Nava, C. Tenailleau, T. Lebey, B. Durand, J.Y. Chane-Ching, Colossal permittivity in ultrafine grain size $BaTiO_{3-x}$ and $Ba_{0.95}La_{0.05}TiO_{3-x}$ materials, Adv. Mater. 20 (2008) 551–555.
[19] U.C. Chung, C. Elissalde, S. Mornet, M. Maglione, C. Estournès, Controlling internal barrier in low loss $BaTiO_3$ supercapacitors, Appl. Phys. Lett. 94 (2009) 072903.
[20] H. Han, D. Ghosh, J.L. Jones, J.C. Nino, Colossal permittivity in microwave-sintered barium titanate and effect of annealing on dielectric properties, J. Am. Ceram. Soc. 96 (2013) 485–490.
[21] A. Artemenko, C. Elissalde, U.C. Chung, C. Estournès, S. Mornet, I. Bykov, M. Maglione, Linking hopping conductivity to giant dielectric permittivity in oxides, Appl. Phys. Lett. 97 (2010) 132901.
[22] H. Han, C. Voisin, S. Guillemet-Fritsch, P. Dufour, C. Tenailleau, C. Turner, J.C. Nino, Origin of colossal permittivity in $BaTiO_3$ via broadband dielectric spectroscopy, J. Appl. Phys. 113 (2013) 024102.
[23] H. Han, C. Davis, J.C. Nino, Variable range hopping conduction in $BaTiO_3$ ceramics exhibiting colossal permittivity, J. Phys. Chem. C (2014) 9137–9142.
[24] C. Voisin, S. Guillemet-Fritsch, P. Dufour, C. Tenailleau, H. Han, J.C. Nino, Influence of oxygen substoichiometry on the dielectric properties of $BaTiO_{3-\delta}$ nanoceramics obtained by spark plasma sintering, Int. J. Appl. Ceram. Technol. 10 (S1) (2013) E122–E133.
[25] D.Q. Nguyen, T. Lebey, P. Castelan, V. Bley, M. Boulos, S. Guillemet-Fritsch, C. Combettes, B. Durand, Electrical and physical characterization of bulk ceramics and thick layers of barium titanate manufactured using nanopowders, J. Mat. Eng. Perf. 16 (2007) 626–634.
[26] C.A. Schneider, W.S. Rasband, K.W. Eliceiri, NIH Image to ImageJ: 25 years of image analysis, Nat. Methods 9 (2012) 671–675.
[27] R.D. Shannon, Revised effective ionic radii and systematic studies of interatomic distances in halides and chalcogenides, Acta Cryst. A 32 (1976) 751–767.
[28] C. Fu, C. Yang, H. Chen, Y. Wang, L. Hu, Microstructure and dielectric properties of $Ba_xSr_{1-x}TiO_3$ ceramics, mater, Sci. Eng. B 119 (2005) 185–188.

[29] L. Zhou, P.M. Vilarinho, J.L. Baptista, Dependence of the structural and dielectric properties of $Ba_{1-x}Sr_xTiO_3$ ceramic solid solutions on raw material processing, J. Eur. Ceram. Soc. 19 (1999) 2015–2020.
[30] G. Caruntu, R. Rarig Jr., I. Dumitru, C.J. O'Connor, Annealing effects on the crystallite size and dielectric properties of ultrafine $Ba_{1-x}Sr_xTiO_3$ ($0 \le x \le 1$) powders synthesized through an oxalate-complex precursor, J. Mater. Chem. 16 (2006) 752–758.
[31] T. Hungria, M. Alguero, A.B. Hungria, A. Castro, Dense, fine-grained $Ba_{1-x}Sr_xTiO_3$ ceramics prepared by the combination of mechanosynthesized nanopowders and spark plasma sintering, Chem Mater. 17 (24) (2005) 6205–6212.
[32] V. Buscaglia, M.T. Buscaglia, M. Viviani, L. Mitoseriu, P. Nanni, V. Trefiletti, P. Piaggio, I. Gregora, T. Ostapchuk, J. Pokorny, J. Petzelt, Grain size and grain boundary-related effects on the properties of nanocristalline barium titanate ceramics, J. Eur. Ceram. Soc. 26 (2006) 2889–2898.
[33] Y. Gao, V.V. Shvartsman, D. Gautam, M. Winterer, D.C. Lupascu, Nanocrystalline barium strontium titanate ceramics synthesized via the organosol route and spark plasma sintering, J. Am. Ceram. Soc. 97 (7) (2014) 2139–2146.
[34] A.K. Jonscher, Dielectric relaxation in solids, J. Phys. D: Appl. Phys. 32 (1999) R57–R70.
[35] A.S. Nowick, B.S. Lim, Electrical relaxations: simple versus complex ionic systems, Phys. Rev. B 63 (184115) (2001) 1–7.
[36] E. Komine, S. Iguchi, Relation of conduction changes and magnetic properties in $Nd_{1-x}Pb_xMnO_3$ ($0.10 \le x \le 0.25$), J. Phys. Cond. Matter 16 (2004) 1061–1073.
[37] R.A. De Souza, C. Voisin, H. Schraknepper, M. Teusner, M. Kessel, P. Dufour, C. Tenailleau, S. Guillemet-Fritsch, Complex diffusion behavior of oxygen in nanocrystalline $BaTiO_3$ ceramics, Phys. Chem. Chem. Phys. 16 (2014) 2568–2575.
[38] R.A. De Souza, V. Metlenko, D. Park, T.E. Weirich, Behavior of oxygen vacancies in single-crystal $SrTiO_3$: equilibrium distribution and diffusion kinetics, Phys. Rev. B 85 (174109) (2012).
[39] S.U. Adikary, H.L.W. Chan, Ferroelectric and dielectric properties of sol–gel derived $Ba_xSr_{1-x}TiO_3$ thin films, Thin Solid Films 424 (2003) 70–74.
[40] M.S. Mohammed, R. Naik, J.V. Mantese, N.W. Schubring, A.L. Micheli, A.B. Catalan, Microstructure and ferroelectric properties of fine-grained $Ba_xSr_{1-x}TiO_3$ thin films prepared by metalorganic decomposition, J. Mat. Res. 11 (10) (1996) 2588–2593.